Advanced Robotics

ISSN: 0169-1864 (Print) 1568-5535 (Online) Journal homepage: www.tandfonline.com/journals/tadr20

Bio-inspired multi-model fusion control for CPG-based quadrupedal locomotion

Jianing Wu, Senwei Huang, Xiuli Zhang & Jiatao Ding

To cite this article: Jianing Wu, Senwei Huang, Xiuli Zhang & Jiatao Ding (13 Sep 2025): Bio-inspired multi-model fusion control for CPG-based quadrupedal locomotion, Advanced Robotics, DOI: 10.1080/01691864.2025.2553102

To link to this article: https://doi.org/10.1080/01691864.2025.2553102

ADVANCED ROBOTICS
https://doi.org/10.1080/01691864.2025.2553102

FULL PAPER

Bio-inspired multi-model fusion control for CPG-based quadrupedal locomotion

Jianing Wu[a], Senwei Huang[a], Xiuli Zhang[a] and Jiatao Ding[b]

[a]The School of Mechanical, Electronic and Control Engineering, Beijing Jiaotong University, Beijing, People's Republic of China; [b]The Department of Cognitive Robotics, Delft University of Technology, Delft, Netherlands

ABSTRACT

Current quadrupedal robot control methods face critical challenges: model-based approaches require extensive manual parameter tuning, while reinforcement learning (RL) methods demand prohibitive training time. To promote quadrupedal robot development, simplify motion controller design, and facilitate robot deployment, this study proposes a novel bio-inspired control scheme. Specifically, inspired by the differentiated modalities of the animal's proximal and distal joints, a multi-model fusion scheme is constructed. First, the hip movement in joint space is obtained by a central pattern generator(CPG), whereby motion gaits, including trotting and galloping, are generated by a coupling network. Then, to generate the knee motion, a CPG-driven finite state machine is first proposed to determine the gait state. On top of this, the spring-loaded inverted pendulum model is utilized to regulate the knee joint's torque command. To enhance forward stability and speed tracking accuracy, this study incorporates online feedback regulation that adjusts both the CPG frequency and joint oscillation amplitude based on attitude angle and forward velocity information. And, a virtual model control strategy is designed to modify the torque profile of the knee torque. To verify the proposed methodology, hardware experiments are conducted on a newly developed quadrupedal robot. Results demonstrate that (i) the small-sized robot can reach 0.8 m/s (2.0 BL/s), with minimal tracking errors and relatively stable robot postures; (ii) compared with the traditional case where CPG generates both hip and knee trajectory directly, the energy consumption is reduced by 11.2% with our method; (iii) the robot can realize smooth trot-gallop-trot gait transition on flat ground and robust walking across uneven terrains.

ARTICLE HISTORY
Received 25 March 2025
Revised 10 June 2025; 13 July 2025; 26 July 2025
Accepted 7 August 2025

KEYWORDS
Bio-inspiration; center pattern generator; multi-model fusion; quadrupedal robot; feedback control

1. Introduction

The research on bionic quadrupedal robots has attracted widespread attention because they have the potential to accomplish dangerous tasks in harsh environments [1–3]. Among various research topics, realizing efficient and robust quadrupedal locomotion is among the prerequisites for deploying the robots in real cases.

The commonly used methods for locomotion control include model predictive control (MPC) [4–6] and whole-body motion control [7–9]. Although effective, the above work requires an accurate physics model. Furthermore, the above work usually relies on numerical optimization for model planning and control, which results in a high computational burden. Also, since there are many optimization parameters that need to be carefully tuned, they usually converge to the suboptimal solution. As an alternative, reinforcement learning (RL) has emerged as a promising solution in recent years [10, 11]. Through interaction with the environment, the control policy can be learned, and dynamic motions can be achieved [12–14]. However, the RL-based methods require millions of iterations and careful tuning of rewards. Besides, the sim2real [15] gap (performance difference between simulation and reality) needs to be addressed.

To tackle the above issues, researchers have proposed to learn from nature, among which the central pattern generator (CPG) [16–19] is widely used to generate rhythmic movements. As a biological neural network with few open parameters, it is able to generate complex movement behaviour. For quadrupedal locomotion, CPG is often utilized to generate swing trajectories (in joint space [20] or task space [21]). In real applications, feedback signals help to regulate the CPG to enhance robustness, improve the traversability, and achieve dynamic motions [22–26].

Nevertheless, the above applications of CPG in quadrupedal robots usually ignore the stiffness variation of different joints. Biological studies indicate that there exist differences in the stiffness of the proximal

CONTACT Xiuli Zhang zhangxl@bjtu.edu.cn; Jiatao Ding jtdingx@163.com

Supplemental data for this article can be accessed online at https://doi.org/10.1080/01691864.2025.2553102.

Table 1. Key parameters used in this article.

Parameters	Definition	Values
m	Mass of 'Feifei'	5.5 kg
l_b	Body length	0.4 m
w_b	Body width	0.32 m
l_1	Thigh length	0.2 m
l_2	Calf length	0.2 m
θ_{hip}	Hip joint angle	/
$\dot{\theta}_{\text{hip}}$	Hip joint angular velocity	/
τ_{knee}	Knee joint torque	/
τ_{hip}	Hip joint torque	/
A	Swing amplitude of the hip joint	/
A_0	The initial value of A	7°
o_x	Equilibrium position of the hip joint swing	45°
l_v	Virtual leg length	/
γ	Yaw	/
D	Duty	$0.3 \sim 0.8$
τ_z	Virtual torque around the Z-axis	/
τ_v	Knee joint torque calculated by VMC	/
τ_s	Knee joint torque calculated by SLIP	/
ω_{stance}	Stance phase frequency	/
ω^0_{stance}	The initial value of ω_{stance}	4π
η	The ratio of swing to stance phase frequency	$D/(1-D)$
ω_{swing}	Swing phase frequency	$\omega_{\text{stance}} \cdot \eta$
T_s	Gait cycle	$\frac{\pi}{\omega_{\text{stance}}} + \frac{\pi}{\omega_{\text{swing}}}$

and distal joints [27–29]. Specifically, the experiments in [28] reveal that the proximal joints (driven by feedforward control) output positive work to promote the forward movement, while the distal joints (behaving as a spring-damper system) reduce the landing impact by absorbing and releasing energy. Furthermore, the proximal movements with higher stiffness can reject external disturbance, while the distal motion is easily changed to accommodate the dynamic uncertainties.

In this paper, we incorporate these biology rules into the quadrupedal control design, aiming at achieving robust and energy-efficient locomotion. To this end, the multi-model fusion (MMF) control scheme is proposed. As shown in Figure 1, the hip movement is directly generated by a CPG planner using a Hopf oscillator [30]. Then, the CPG-driven finite state machine (C-FSM) is designed to modulate the knee movement, on top of which the spring-loaded inverted model (SLIP) [31] and virtual model control (VMC) [32] are integrated to generate the compliant knee torque. To enhance robustness, we regulate CPG behaviour using sensory feedback (attitude angles and forward velocity) to modulate both CPG oscillation frequency and joint movement amplitude. Furthermore, we dynamically adjust: (1) coupling phases between CPG units, (2) joint equilibrium positions, and (3) virtual leg lengths in the SLIP model. These coordinated adjustments enable seamless trot-gallop-trot transitions and adaptive obstacle negotiation on challenging terrains.

Our main contributions are threefold:

- A CPG network with feedback regulation is introduced to generate reactive hip movement, endowing the proximal joint with higher stiffness.
- On top of the C-FSM, the SLIP, together with VMC, is used to generate torque command of the knee joint, realizing reactive and compliant distal movement.
- Hardware experiments in a newly designed quadruped demonstrate the stable, robust, and energy-efficient locomotion with the proposed approach.

In the rest, Section 2 briefly introduces the proposed approach. Section 3 details the bio-inspired MMF method. Section 4 presents the experimental results, and Section 5 concludes this work.

2. Overall

The overall flow of the proposed bio-inspired MMF control is illustrated in Figure 1.

The basic modules (green blocks) of this framework consist of a CPG and a C-FSM. In particular, the CPG generates the swing trajectory of the hip joint (denoted by θ_{hip} in Figure 1), whose motion is tracked by a PD controller. Then, according to the hip's joint position and angular velocity, the C-FSM decides whether the leg is in the stance or swing phases.

Then, knee joint torque control (the blue blocks) is achieved by fusing two parts. One part is obtained by utilizing the SLIP model, which ensures contact compliance, while the other part is derived from the VMC, which guarantees postural stability.

Finally, to enhance robustness, feedback control (yellow blocks) adjusts the characteristic parameters of the CPG and the control output of VMC according to the real state and the task requirements. In this work, we adopt a Kalman filter-based foot odometry approach [33] to estimate the robot's state, particularly its forward velocity and trunk attitude angles. The detailed implementation follows and will not be elaborated here.

As a preliminary validation, we work with a newly-design quadruped with 8 actuated joints, including a hip and a knee joint on each leg. A detailed introduction of the hardware platform can be found in Section 4.1.

3. Bio-inspired multi-model fusion control

In this section, we provide a detailed explanation of how our framework generates gait, ensures compliance during the stance phase, and adapts to environmental uncertainties. Without specific explanation, symbols are defined in Table 1.

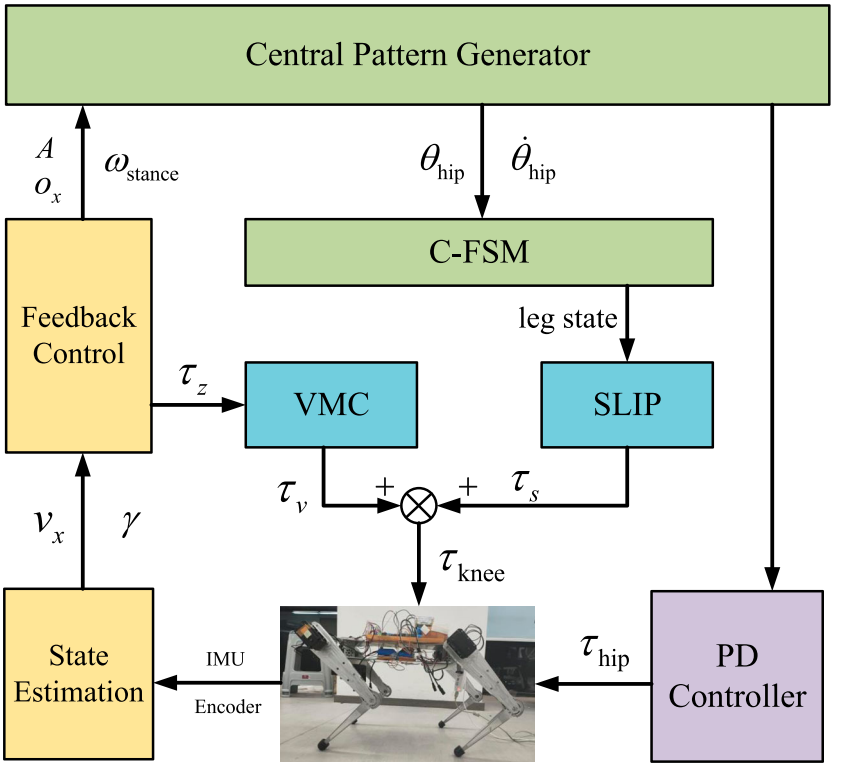

Figure 1. The proposed control pipeline. The CPG generates hip motion (in joint space) directly while the C-FSM coordinates knee status. The sensory feedback (orange) determines parameters for CPG and torque input for VMC. Combining VMC with SLIP, compliant knee motion is achieved in torque control mode. The operating frequency of the control algorithm is 100 Hz. Other symbols are defined in Table 1.

3.1. CPG-based gait generation

A CPG network is introduced to generate the proximal joint motion with high stiffness. In this work, a Hopf oscillator [30] is used as a basic unit of the CPG network, but we reduce the coupling strength to simplify computation. With symbols defined in Table 2, the hip movement is generated by

$$\begin{aligned} \dot{x} &= \alpha(\mu^2 - r^2)x - \omega y, \\ \dot{y} &= \delta(\mu^2 - r^2)y + \omega x, \\ \omega &= \frac{\omega_{\text{stance}}(e^{by} + \eta)}{e^{by} + 1}, \\ r^2 &= x^2 + y^2. \end{aligned} \tag{1}$$

In Table 2, φ_0^i denotes the phase difference between the i-th ($i \in \{1, \ldots, 4\}$) oscillator and the reference oscillator (No. 0). The indices $i = 1, 2, 3, 4$ denote the left front leg (LF), right front leg (RF), left hind leg (LH), and right hind leg (RH), respectively. The CPG coupling network, which includes both φ_0^i and the phase difference between the left and right legs (denoted as φ_{LR}) is depicted in Figure 2. In particular, the coupling relationship between

Table 2. Parameters of the Hopf oscillators.

Parameters	Definition	Values
x, y	Output of the oscillator	$-1 \sim 1$
μ	Amplitude of oscillator	1
α	The convergence factor of x	3
δ	The convergence factor of y	3
b	Constant of integration	100
e	Natural exponential	2.7183
k	Coupling factor	1
r	Limit cycle radius	1
ω	Oscillator frequency	/
φ_i^0	Phase difference	/
φ_{LR}	Left-right leg phase difference	/

Hopf oscillators is defined as

$$\begin{aligned} \dot{x}_0 &= \alpha(\mu^2 - r_0^2)x_0 - \omega y_0, \\ \dot{y}_0 &= \delta(\mu^2 - r_0^2)y_0 + \omega x_0, \\ \dot{x}_i &= \alpha(\mu^2 - r_i^2)x_i - \omega y_i + k(x_0 \cos\varphi_0^i - y_0 \sin\varphi_0^i), \\ \dot{y}_i &= \delta(\mu^2 - r_i^2)y_i + \omega x_i + k(x_0 \cos\varphi_0^i + y_0 \sin\varphi_0^i). \end{aligned} \tag{2}$$

However, the desired trajectory generated by (2) can be counterintuitive due to the constrained output signal within a narrow range. In this work, we opt to scale and translate the CPG initial output value to achieve an appropriate trajectory for the hip joint of the i-th leg,

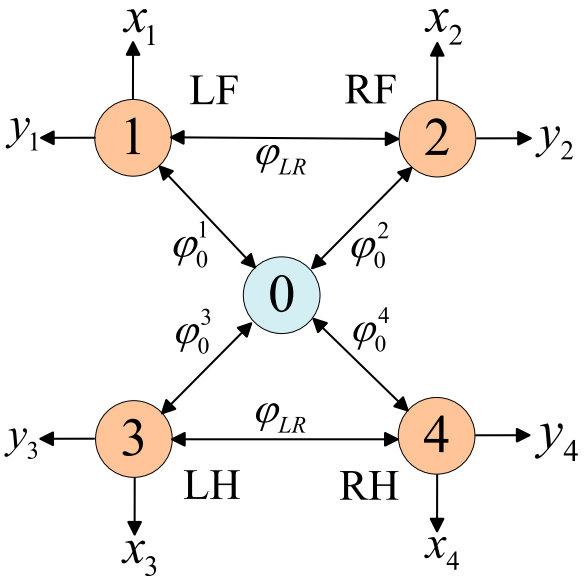

Figure 2. Gait generation based on φ_0^i and φ_{LR}. For the trot gait, $[\varphi_0^1, \varphi_0^2, \varphi_0^3, \varphi_0^4] = [0, \pi, \pi, 2\pi]$, $\varphi_{LR} = \pi$, and $\varphi_0^2 = \varphi_0^1 + \varphi_{LR}$, $\varphi_0^4 = \varphi_0^3 + \varphi_{LR}$. x_i and y_i can be used to generate the swinging trajectories of the hip and knee joints. In this work, only the hip trajectory (generated by x_i) is utilized.

following

$$\theta_{\text{hip}}^i = Ax_i + o_x. \tag{3}$$

To intuitively understand the relationship between CPG behaviour and hip joint trajectories, Figure 3 presents an example plotted according to (3), where A and o_x are set to 10° and -45°, respectively.

To track the desired speed, ω_{stance} is regulated online by

$$\omega_{\text{stance}} = \omega_{\text{stance}}^0 + k_\omega(v_d - v_x), \tag{4}$$

where k_ω, v_d, v_x are the coefficient, the desired speed and the actual speed, respectively.

Another advantage is that the above CPG-based model enables smooth gait transitions by adjusting the coupling phase. For example, the phase differences for trot and gallop gaits are $[\varphi_0^1, \varphi_0^2, \varphi_0^3, \varphi_0^4] = [0, \pi, \pi, 2\pi]$ and $[0, \pi/2, \pi, 3\pi/2]$, respectively. The transition between trot and gallop is controlled by the phase shift between the left and right legs, following,

$$\varphi_{LR} = \varphi_{LR}^0 + \chi \frac{\pi}{2t_p}(t - t_s), \tag{5}$$

where φ_{LR}^0 is the initial phase difference, which depends on the gait prior to the transition. χ represents the conversion direction, with a value of 1 indicating a transition from gallop to trot and -1 indicating a transition from trot to gallop. t_p, t, and t_s denote the conversion duration, the current time, and the start time, respectively.

Table 3. Parameters such as stiffness and damping in the SLIP model.

Phase	Stifness[N/m]	Damping[Ns/m]	F_{thrust}[N]
Flight	60	0.6	/
Compression	80	0.8	0
Thrust	100	1	5

3.2. SLIP-based compliance control

Inspired by the low stiffness property and high stance compliance found in the distal joints of animals, we employ a simplified SLIP model, which focuses solely on the compression and extension control of the virtual spring-loaded leg in quadrupedal robots, to regulate the torque profile of the knee joint. Within this model, the leg states are intricately coupled with the swing trajectory of the hip joint and can be categorized into three phases: flight, compression, and thrust [17–19]. As illustrated in Figure 4, when the angular velocity of the hip joint is negative, i.e. $\dot{\theta}_{\text{hip}} < 0$, the single leg is in the swing phase. Conversely, when the angular velocity is positive, the leg switches into the stance phase. When touching the ground, if the hip joint is positioned before the equilibrium point ($\theta_{\text{hip}} < o_x$), the leg enters the compression phase. Otherwise, if the hip joint is positioned beyond the equilibrium point, the leg enters the thrust phase.

After determining the leg status, the SLIP model is used to achieve compliant motion, whereby the spring force (F_s in Figure 5) is regulated online by incorporating sensory feedback. As illustrated in Figure 5, during the stance phase, the spring force is determined by

$$F_s = k_s^p(l_v - l_s^0) + k_s^d\dot{l}_v + F_{\text{thrust}}. \tag{6}$$

During the swing phase, we have

$$F_s = k_f^p(l_v - l_f^0) + k_f^d\dot{l}_v. \tag{7}$$

In (6) and (7), F_{thrust} is the supplementary thrust, which is zero during the compression phase and is adjusted during the thrust phase. k_s^p, k_s^d, k_f^p, and k_f^d are the stiffness and damping coefficients for the stance and swing phases, respectively, as shown in Table 3. Their values are manually adjusted based on experimental results to optimize performance [31]. l_v, calculated through kinematics, represents the distance between the foot and the single-leg coordinate origin. $\dot{l}_v$ denotes the change rate of l_v. The initial values of l_v in the stance and swing phases are set as l_s^0 and l_f^0, respectively, which are manually adjusted.

To obtain the desired torque for the knee joint, F_s is first decomposed into

$$\begin{aligned} F_x &= F_s \sin(\theta_{\text{hip}} - \theta_{\text{vir}}), \\ F_z &= F_s \cos(\theta_{\text{hip}} - \theta_{\text{vir}}), \end{aligned} \tag{8}$$

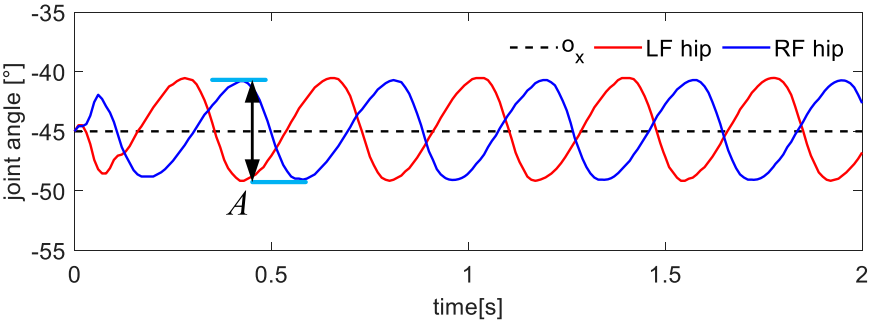

Figure 3. The CPG behaviour is mapped to the hip joint trajectory signals. Taking the LF and RF legs in the trot gait as examples, the dashed line represents the hip joint's equilibrium position–the midpoint between the anterior and posterior extreme positions. The initial value of the trajectory signal in the figure is in an unstable state, which is caused by the inconsistency of the initial states of the oscillator signals. However, it can converge to a stable signal in a short time and will not affect the subsequent movement.

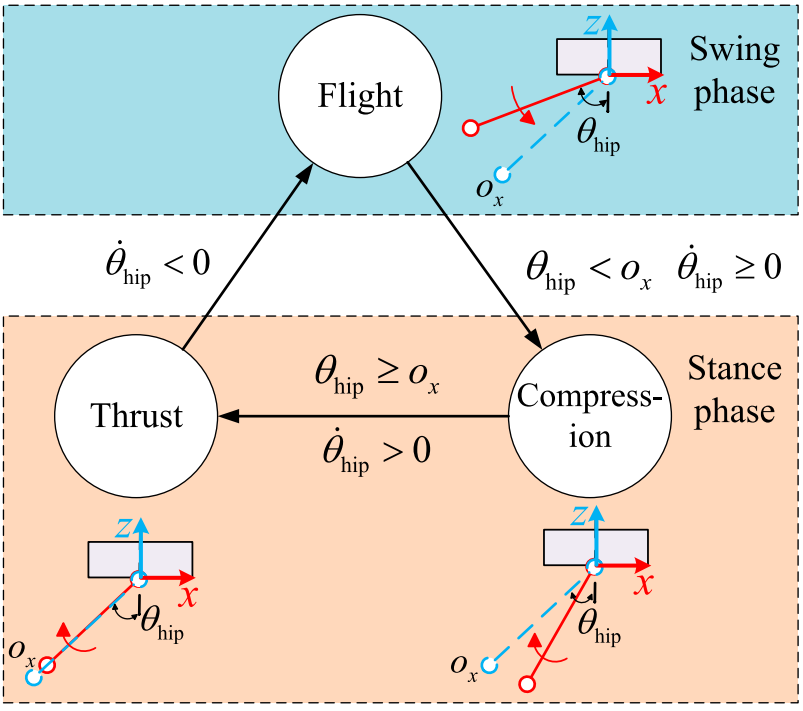

Figure 4. Phase switch via the C-FSM. The blue dashed line indicates the equilibrium position of the hip joint, while the red solid line represents the actual hip position.

where F_x and F_z are separately the forward and vertical forces, θ_{vir} is the angle between the virtual leg and the thigh (see Figure 5).

Then, the leg torque $\boldsymbol{\tau}_l \in \mathbb{R}^2$ resulting from the SLIP model is determined by

$$\boldsymbol{\tau}_l = -\boldsymbol{J}^{\mathrm{T}}\boldsymbol{F}, \tag{9}$$

with $\boldsymbol{F} = [F_x, F_z]^{\mathrm{T}}$, $\boldsymbol{\tau}_l \in \mathbb{R}^2$ is the joint torques and $\boldsymbol{J} \in \mathbb{R}^{2\times 2}$ is the contact Jacobian. Here, we only use the knee component, denoted as $\boldsymbol{\tau}_s$ in Figure 1.

Note that, in the SLIP model, the lift height during the swing phase is adjusted according to the expected length of the virtual leg l_f^0. It should be noted that the height of the obstacle is measured in advance and known. As illustrated in Figure 6, when walking across step-like terrain, l_f^0 is set to $\hat{l}_f^0$ according to the obstacle height, and the hip joint balance position o_x is adjusted to $\hat{o}_x$ to lower the body height. These changes improve the robot's traversability across obstacles.

$$\begin{aligned} \hat{l}_f^0 &= l_f^0 - \frac{(l_f^0 - \hat{l}_f^0)}{t_{ds}}t, \\ \hat{o}_x^0 &= o_x^0 - \frac{(o_x^0 - \hat{o}_x^0)}{t_{ds}}t, \end{aligned} \tag{10}$$

In (10): l_f^0 and o_x^0 are the initial desired virtual leg length for swing phase and the hip joint equilibrium position;

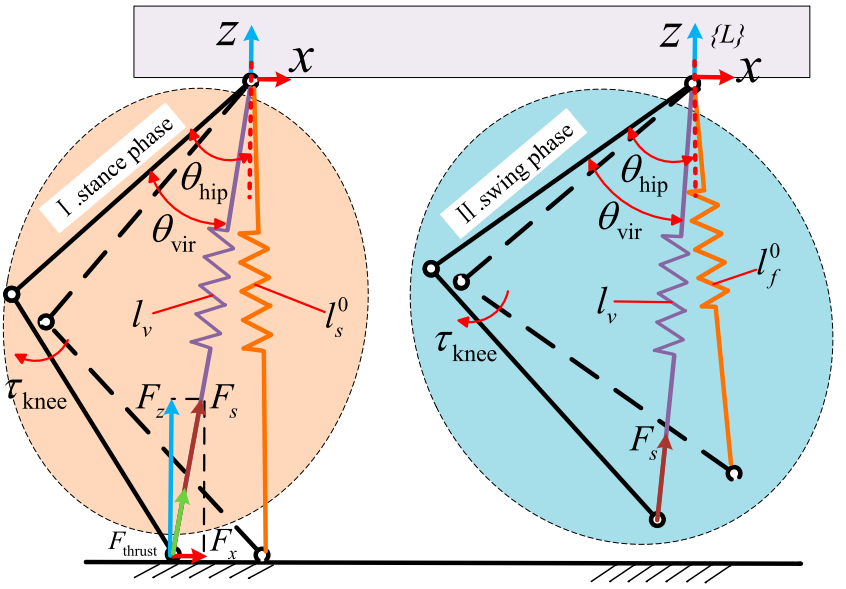

Figure 5. I and II represent the stance phase and the swing phase, respectively. The orange line represents the original length of the virtual leg, while the purple one represents the actual virtual leg length. The green arrow indicates the supplementary thrust force F_{thrust}.

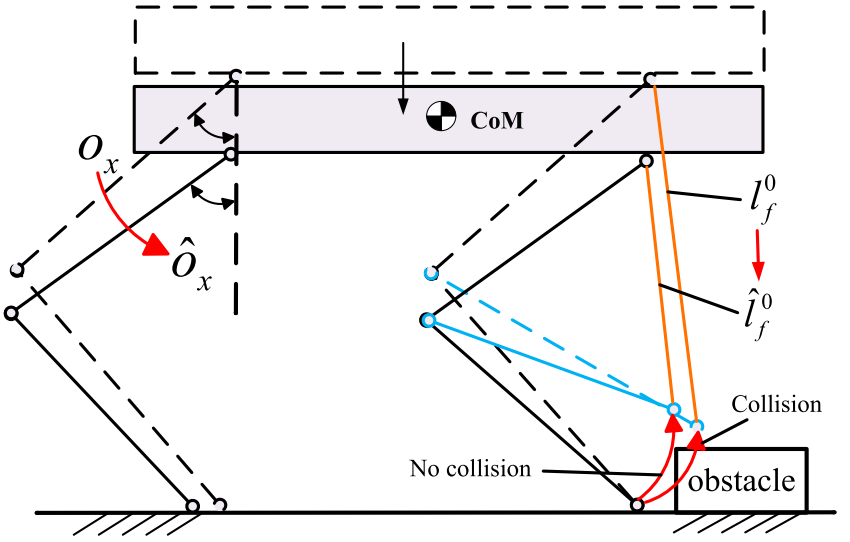

Figure 6. Lift height modulation when walking across uneven terrain. The dotted lines represent the normal operating state, and the solid lines represent the state that is more likely to pass obstacles. $\hat{o}_x$ and $\hat{l}_f^0$ are the modulated balanced position of the hip joint and the expected swing virtual leg length, which are changed according to the actual height of the obstacle.

$\hat{l}_f^0$ and $\hat{o}_x^0$ are the adjusted virtual leg length during the swing phase and the joint equilibrium position when facing obstacle terrain, with values of 0.255 m and -50° respectively in the experiment; t_{ds} is the desired transition time, with a value of 0.4 s, and t is the starting time point for the transition.

3.3. Posture stability control

To realize fast walking while maintaining a stable posture, this section designs a direct feedback control strategy utilizing motion information obtained through state estimation. To this end, several factors are taken into consideration.

3.3.1. VMC

This robot lacks a lateral swing joint and thus can not directly regulate yaw behaviour when yaw deviations occur. To solve this issue, we utilize VMC to adjust the robot's posture angle. The torque command for yaw reduction is generated by

$$\tau_z = k_\gamma (\gamma_d - \gamma). \tag{11}$$

where k_γ is the coefficient, γ_d is the desired yaw angle.

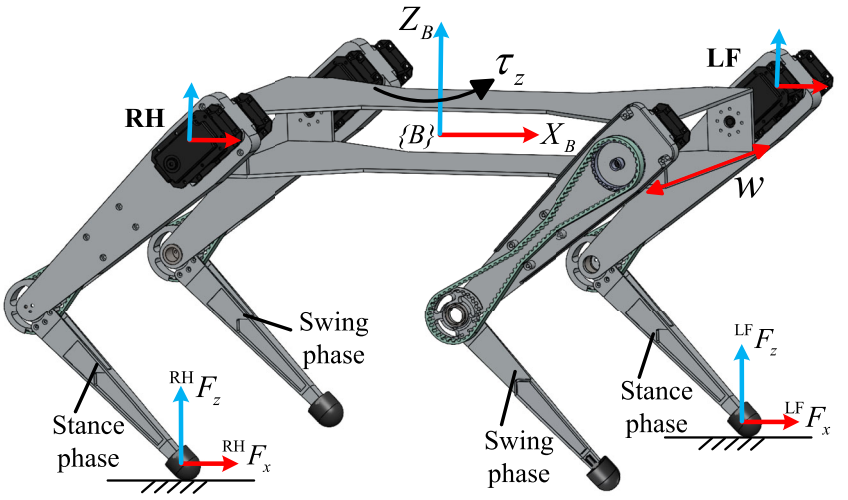

Figure 7. The robot trots with the LF and RH legs in the stance phase and the RF and LH legs in the swing phase.

The trotting motion depicted in Figure 7 shows that the vertical foot along the Z-axis direction aligns with the Z_B-axis. Consequently, only the component of the reactive force along the X axis contributes to the virtual yaw moment. To assign τ_z to the foot end force, we introduce an adjustment factor s that allows for the regulation of the force distribution ratio between the left and right legs. Taking the Figure 7 for example, the foot end force is regulated as

$$\begin{aligned} {}^{\mathrm{LF}}F_x &= \frac{2\tau_z}{w_b}\cdot\frac{1}{s}, \quad {}^{\mathrm{LF}}\boldsymbol{F}_{\mathrm{yaw}} = [{}^{\mathrm{LF}}F_x, 0]^T, \\ {}^{\mathrm{RH}}F_x &= \frac{2\tau_z}{w_b}\cdot\frac{s-1}{s}, \quad {}^{\mathrm{RH}}\boldsymbol{F}_{\mathrm{yaw}} = [{}^{\mathrm{RH}}F_x, 0]^T. \end{aligned} \tag{12}$$

where ${}^{\mathrm{LF}}F_x$ and ${}^{\mathrm{RH}}F_x$ are the sagittal force in the LF and RH legs, ${}^{\mathrm{LF}}\boldsymbol{F}_{\mathrm{yaw}}$ and ${}^{\mathrm{RH}}\boldsymbol{F}_{\mathrm{yaw}}$ are the yaw reduction forces in the LF and RH legs.

By substituting $\boldsymbol{F}_{\mathrm{yaw}}$ into (9), the posture adjustment torque τ_v is obtained through the mapping of $\boldsymbol{J}$.

Ultimately, the knee joint torque τ_{knee} is determined as

$$\tau_{\mathrm{knee}} = \tau_s + \tau_v. \tag{13}$$

3.3.2. Hip joint amplitude

To reduce yaw while tracking the desired speed, we modulate the swing amplitude, following

$$A = A_0 + \delta k_A(\gamma_d - \gamma) + k_b(v_d - v_x), \tag{14}$$

where k_b is the coefficient for velocity tracking, k_A is the coefficient for yaw reduction. Here, δ is 1 for the left leg and -1 for the right leg.

4. Experimental results

To demonstrate the effectiveness, we conducted experiments on the quadrupedal robot 'Feifei', whose physical parameters are detailed in Table 1. The extensive experiments include stable and efficient locomotion, speed tracking, gait transitions, and walking across uneven terrain. All the experiments can be found at https://youtu.be/EglSolXh5CM.

4.1. Robot system

'Feifei' is fabricated with Aluminum alloy and offers 8 DOFs. Thanks to its efficient joint drive system, which utilizes MX-106 servos, position and torque commands can be executed simultaneously by two actuators on each leg. Additionally, the system provides information on the joint position, and electrical current. The control algorithm runs at 100 Hz on the Raspberry Pi 4B, communicating with the servos via the STM32 microcontroller. A physical prototype of 'Feifei' is illustrated in Figure 8.

4.2. Stable and efficient walking

To start with, we verify locomotion performance with different walking parameters. In particular, we compare the proposed MMF control approach with the conventional CPG method [30], where all joint trajectories are directly generated by oscillators without the VMC feedback regulation described in Section 3.3.1.

With the traditional CPG method, the swing amplitude of the robot's hip joint was set to 8°, and the knee joint amplitude was 16°–values empirically determined through iterative hardware testing to ensure stability within the operational parameter range. The knee joint

Table 4. Parameters setting of CPG and MMF in walking experiments.

Method	Hip amplitude [°]	Knee amplitude [°]	Virtual leg length [m]	ω_{stance} [rad/s]
CPG	8°	16°	/	$4\pi, 5\pi, 6\pi$
MMF	8°	/	0.3 m in stance phase 0.26 m in swing phase	$4\pi, 5\pi, 6\pi$

Figure 8. The quadrupedal robot 'Feifei'.

Table 5. At a duty cycle of 0.5, mean and MSE of yaw under different CPG and MMF parameters.

Method	Joint amplitude	ω_{stance}	Mean	MSE
CPG	$h = 6°, k = 12°$	4π	0.055	0.005
MMF	$h = 6°$	4π	**0.005**	**0.001**
CPG	$h = 8°, k = 16°$	4π	0.028	0.001
MMF	$h = 8°$	4π	**−0.025**	0.002
CPG	$h = 10°, k = 20°$	4π	−0.015	0.001
MMF	$h = 8°$	4π	−0.063	0.005
CPG	$h = 6°, k = 12°$	5π	0.103	0.015
MMF	$h = 6°$	5π	**0.054**	**0.004**
CPG	$h = 8°, k = 16°$	5π	0.113	0.021
MMF	$h = 8°$	5π	**−0.096**	**0.012**
CPG	$h = 10°, k = 20°$	5π	−0.059	0.004
MMF	$h = 10°$	5π	**0.025**	**0.002**
CPG	$h = 6°, k = 12°$	6π	−0.001	0.001
MMF	$h = 6°$	6π	−0.146	0.029
CPG	$h = 8°, k = 16°$	6π	0.125	0.023
MMF	$h = 8°$	6π	−0.204	0.051
CPG	$h = 10°, k = 20°$	6π	0.070	0.009
MMF	$h = 10°$	6π	−0.108	0.013

swing amplitude in CPG theoretically approximates the variation range of virtual leg length in stance and swing phases of MMF. The MMF method does not directly specify the swing amplitude of the knee joint. Instead, the desired swing angle of the knee joint is indirectly determined by setting the desired virtual leg lengths in the stance phase and swing phase. According to the lengths of the thigh and shank, as well as the virtual leg length, the desired angles of the knee joint in the stance phase and swing phase are calculated using the Law of Cosines to be 97.18°c and 81.08°, respectively. The resulting knee joint swing amplitude is exactly 16.1°, which corresponds to the CPG method in Table 4. Based on this, we performed multiple sets of experiments at various swing frequencies and duty cycles. For simplicity, we evaluate the yaw motion, as the roll and pitch exhibit similar behaviour. As illustrated in Figure 9, the MMF method demonstrates better stability, i.e. with less yaw, due to the direct feedback regulation. Furthermore, when the deviation occurs, our method effectively corrects it, bringing the yaw angle back to zero. In contrast, the traditional CPG method tends to diverge. To qualitatively demonstrate the stability advantages of MMF, multiple sets of experiments with different joint amplitudes and swing frequencies were conducted. Each group of experiments in Table 5 was repeated 2 times with a duration of 8 seconds, where the desired yaw angle was consistently 0°. The mean and mean squared error (MSE) of yaw were calculated, and the results are presented in Table 5. Notably, when the swing frequency was 5π, both the mean value and MSE of the yaw angle for MMF were smaller than those for traditional CPG. Consequently, the swing frequency was set near 5π in subsequent experiments.

Additionally, the robot using the naive CPG method exhibited a foot-dragging phenomenon in the locomotion (see Figure 10), resulting in lower forward speed and higher landing impact. Although parameter tuning of the CPG could theoretically mitigate this issue, such adjustments demonstrated limited effectiveness in our robotic platform due to inherent hardware constraints. As a result, the real forward speed of MMF is significantly faster than that of CPG when using different swing frequencies and amplitudes. For example, when the duty cycle is 0.5, compared with CPG, the speed can be increased by at least 10%. Notably, this performance gap amplifies proportionally with higher oscillation frequencies. The velocity profiles are compared in Figure 11.

In addition to stable walking, we also compare the energetic performance and knee joint compliance when using the above two methods. To this end, we conducted trotting experiments involving a forward movement of 2 m, repeating three times with $\omega_{\text{stance}} = 5\pi$, $A_0 = 8°$, $D = 0.5$. In this study, we calculated the average output power and energy consumption by utilizing the measured joint torque and angular velocity, and computed the average input power using measured voltage and current values. The average energy consumption is reported in Table 6, showing that the MMF method achieves an average reduction of 11.2%. The energy reduction is attributed to the SLIP control of the knee joint, which effectively mitigates foot-dragging on the ground by

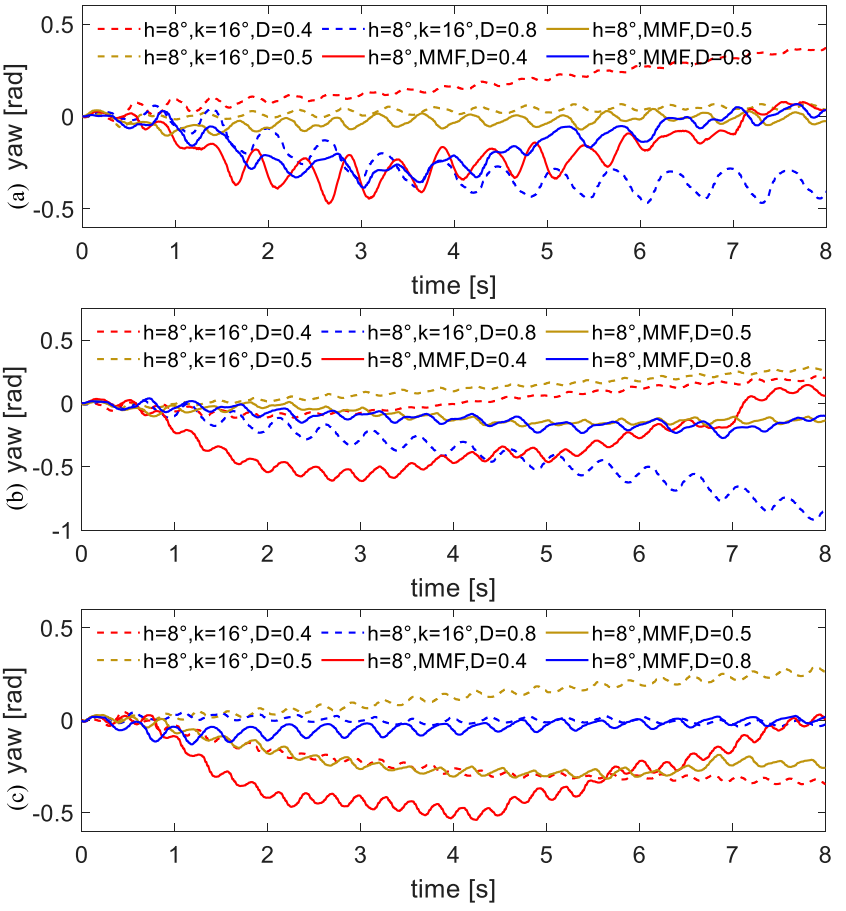

Figure 9. Yaw behaviour with different methods under different parameters. 'h', 'k', and 'D' denote the hip amplitude, knee amplitude, and duty cycle, respectively. (a), (b), and (c) plot the real yaw angles with ω_{stance} being 4π, 5π, and 6π, respectively.

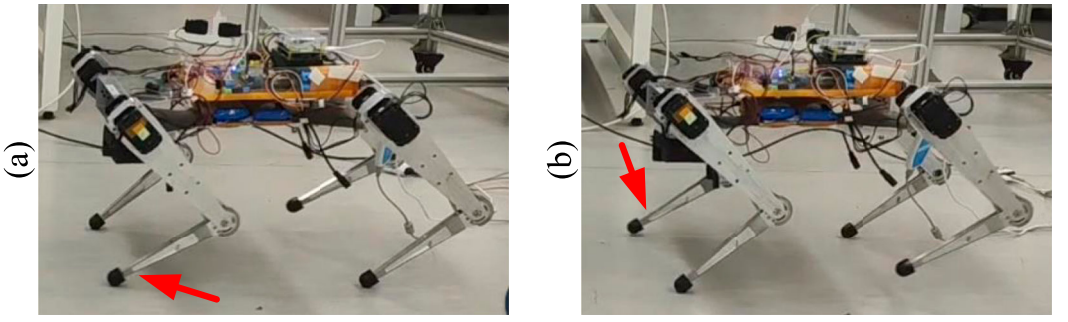

Figure 10. The traditional CPG method causes the foot to drag on the ground. (a) The LF leg should be lifted now. (b) The RF leg should be lifted now.

prescribing a desired virtual leg length. Additionally, its compliant force contributes to reducing foot-ground impact.

Since there are no foot force sensors on the robotic platform, we validated our method's distal compliance using the actual torque of the knee joint, as illustrated in Figure 12. As can be seen, when the robot's leg moves from the swing phase to the stance phase (when the 'state' plot jumps from 0 to 1), the foot makes contact with the ground, causing fluctuation in the torque at the knee joint. Notably, while the MMF method generally produces lower knee joint torque during the stance phase, the higher torque observed in the MMF swing phase is a normal phenomenon: it arises because the SLIP model calculates knee torque based on virtual leg length, and the large deviation between the desired position and the current position at the initial swing phase triggers this transient increase. This characteristic of MMF contributes to its enhanced obstacle traversal capability, as the greater torque during the swing phase facilitates

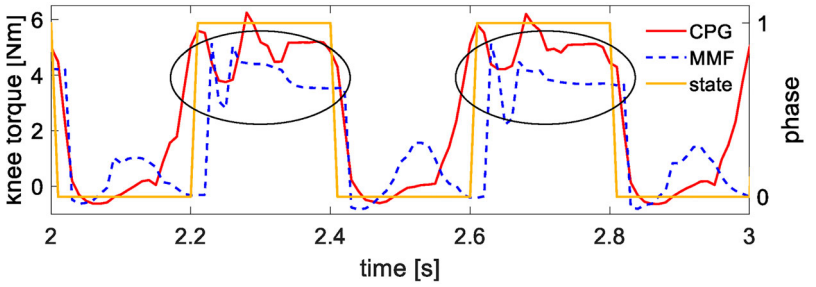

Figure 11. Real forward speed when using different methodologies. (a), (b) and (c) show the results with ω_{stance} being 4π , 5π , and 6π respectively.

Table 6. The average energy consumption of forward trotting.

Method	Movement time [s]	Consumption [J]	Output power [W]	Input power [W]
CPG	6.03	711.5	8	118
MMF	**5.03**	**593.5**	**9.5**	118

more effective leg lifting. However, the MMF method produces lower knee joint torque compared to the CPG method, as shown in the highlighted areas. The CPG-based FSM is fundamentally similar to traditional time-series state machine switching in quadruped robots, as CPG trajectory generation functions include time variables with phase coupling between oscillators. Since C-FSM's single-leg motion states are also time-dependent, tracking errors inevitably occur. For instance, when C-FSM dictates a transition from swing to stance phase, motor delays or body vibrations can disrupt foot placement, causing delays in actual state transitions.

4.3. Velocity tracking

To evaluate the velocity tracking performance, we controlled the robot to follow a step-velocity profile. As shown in Figure 13(a), the desired velocities (red line) at 0 to 4 s, 4 to 8 s, and 8 to 12 s were 0.6 m/s, 0.7 m/s, and 0.8 m/s, respectively. It can be observed that the robot (blue curve) is capable of adapting to the velocity variation within a short period and achieving a small static error. Figure 13(b–d) respectively show the joint swing frequencies, LH joint amplitude, and RH joint amplitude. In addition, Figure 13(e) demonstrates that the roll and pitch angles are well-controlled between −0.05 rad and 0.05 rad throughout the process.

The results demonstrate that 'Feifei' is capable of steadily trotting at a speed of 0.8 m/s (2 BL/s, where BL denotes Body Lengths per second). Given the relatively small leg size of the robot, this achieved speed is notable. The detailed motion can be found in the attached video.

4.4. Gait transition

Due to the utilization of CPG, our MMF method can easily realize gait transitions by adjusting the phase difference φ_{LR} between the left and right legs (as shown in (5)). Gait transition is crucial for animals when accelerating to chase prey. Figure 14 shows the transition from trot to gallop and back to trot.

The phase differences for trot and gallop are represented as $\varphi_{\text{trot}} = [0, \pi, \pi, 2\pi]$ and $\varphi_{\text{gallop}} = [0, \pi/2, \pi, 3\pi/2]$, respectively. The phase of the hip joint reflects the gait transition process, as shown in Figure 15. Due to the online adjustment in the yaw motion and ground shocks in the position loop, the tracking performances of the left and right joint angles are different. However, the phase variations of the left and right legs conform to expectations.

4.5. Walking across uneven terrain

This section evaluates the adaptability of the MMF to uneven terrain by adjusting the equilibrium position of the hip joint and the virtual leg length to accommodate the actual height of the obstacles. In the experiment, the obstacle height was approximately 2 cm and pre-known. The middle equilibrium position of hip joint swing and the virtual leg length of the knee joint in MMF were manually adjusted according to the actual obstacle height to cross the obstacle. As illustrated in Figure 16, the naive CPG method, without adjusting the equilibrium position and the virtual leg length, becomes obstructed by obstacles, while the MMF demonstrates stronger traversability. The same adjustment idea cannot achieve the same effect in the CPG method, as the front legs dragging on the ground make it difficult for the robot to cross the obstacle.

Figure 17 details the locomotion trajectories with the change in the equilibrium position. As shown in Figure 17(a,b), the equilibrium position of the robot's hip joint is adjusted to stabilize the robot, as it helps lower the center of mass. Additionally, during the swing phase,

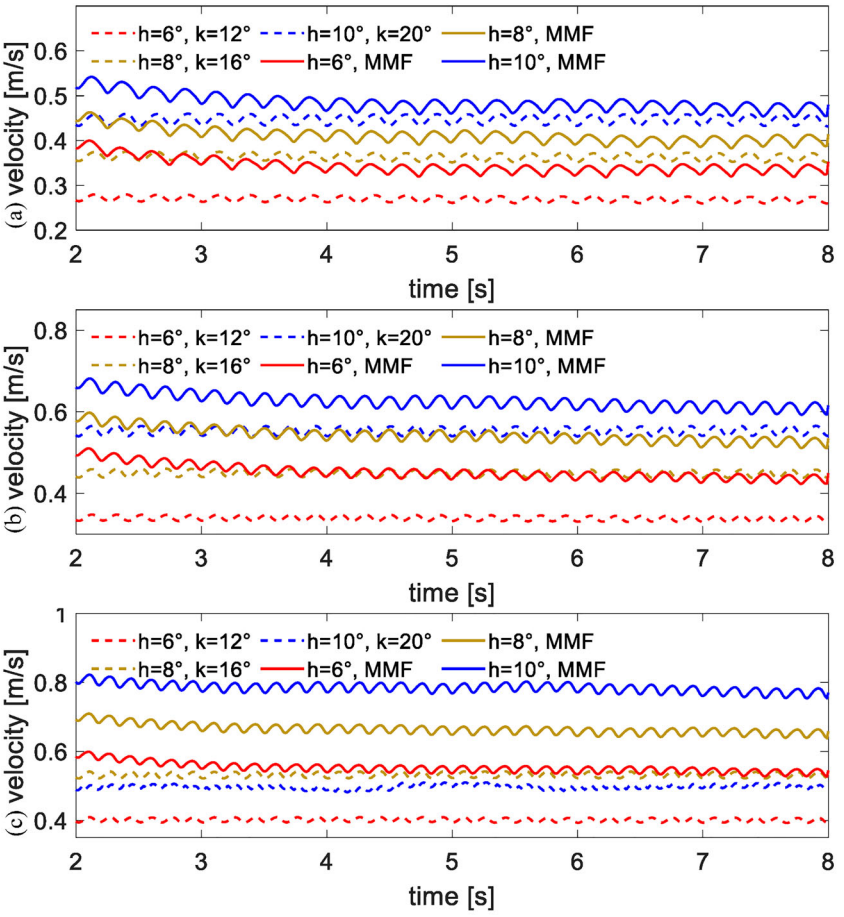

Figure 12. The actual knee joint torque of the LF leg. The yellow line indicates the leg's phase state, where a value of 1 represents the stance phase and a value of 0 represents the swing phase.

the virtual leg length decreases, as illustrated in Figure 17(c,d). At 2.5 s, the robot steps onto the platform, which causes significant fluctuations in its posture, as can be seen in Figure 17(e). The black dashed lines indicate the moments when the robot steps onto and leaves the platform. Additionally, between 3 and 6 s, the robot's roll angle reaches the maximum (0.14 radians), while the pitch reaches −0.15 radians. This adjustment causes the robot's center of gravity to shift toward the right hind leg, leading to a pronounced compression of the virtual leg length for that leg, as illustrated in Figure 17(d). After 6 s, the robot passes across the platform, and its posture gradually stabilizes.

5. Discussion

The proposed bio-inspired multi-model fusion (MMF) control scheme effectively addresses the limitations of traditional CPG-based approaches by integrating biological insights into robotic locomotion. By distinguishing the roles of proximal (hip) and distal (knee) joints–modelling the hip as a high-stiffness actuator driven by CPG and the knee as a compliant component regulated by SLIP and VMC–the framework achieves a balance between stability and energy efficiency. The hardware experiments validate that MMF reduces energy consumption by 11.2% compared to conventional CPG methods, primarily due to the SLIP model's ability to mitigate foot-dragging and impact forces during stance phases [31].

In the method, the C-FSM determines the movement phase of a single leg based on the hip joint trajectory signals generated by the CPG. This provides a switching mechanism for the knee joint's force control model, enabling the dynamic generation of knee joint torque commands for the single leg. While the C-FSM coordinatesthe movement of a single leg in a simple and effective manner, it also has instability issues. For example, there is a delay between the real stance phase and the stance phase determined by the C-FSM.

The online feedback regulation of CPG frequency and joint amplitude based on velocity and attitude angles demonstrates the method's adaptability to dynamic environments. For instance, the robot maintains stable yaw

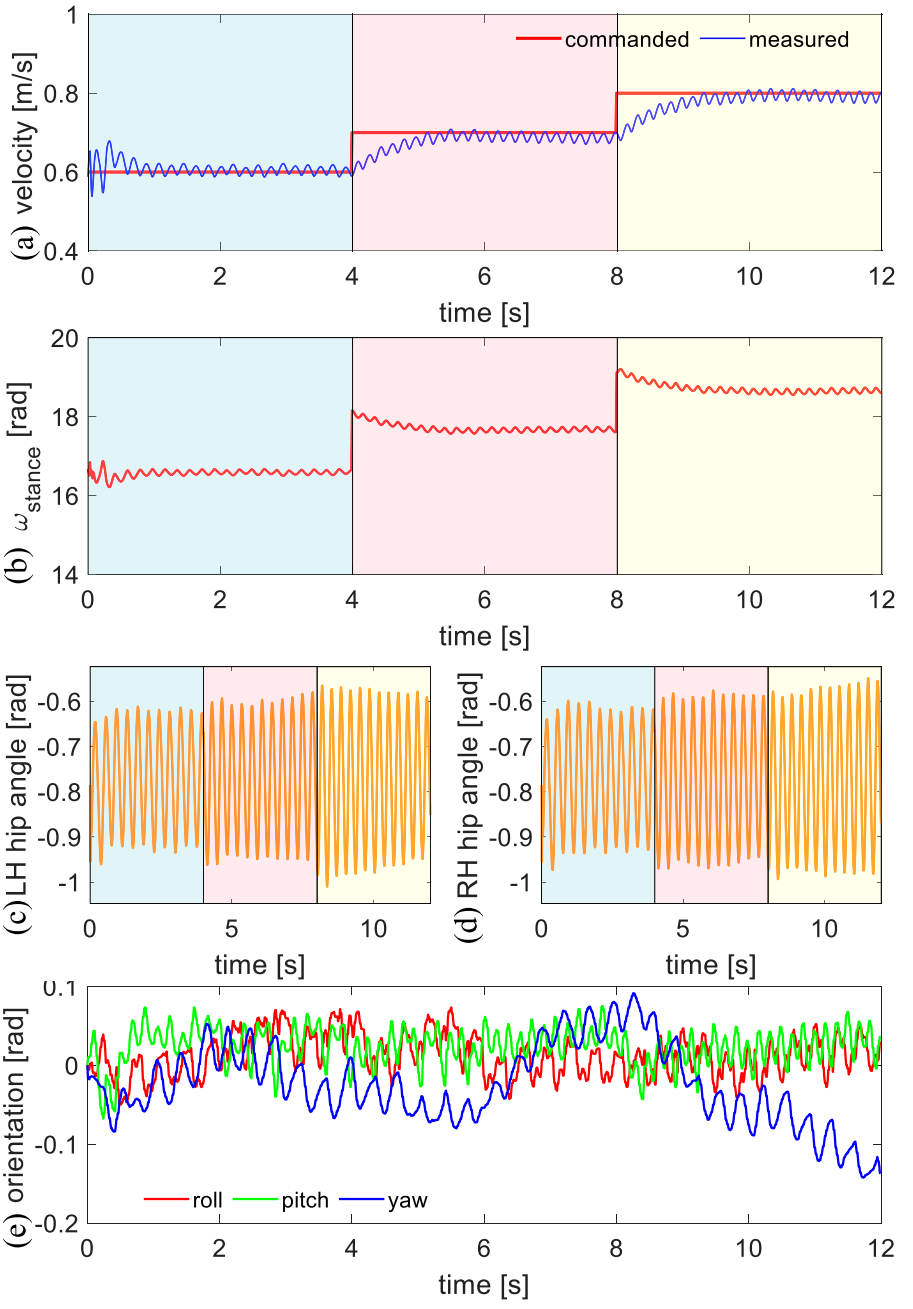

Figure 13. Velocity tracking performance: (a) Step speed following. (b) Swing frequency of the hip joint in the stance phase. (c) Hip angle of the LH leg. (d) Hip angle of the RH leg. (e) Body orientation.

angles within ±0.05 rad during speed tracking up to 0.8 m/s, a performance attributed to the VMC's corrective torque (12) and the CPG's phase adjustment mechanism (14). However, MMF has certain limitations and can only exhibit a more stable motion model within a specific parameter range. For example, as shown in Table 5, MMF does not outperform the traditional CPG under all parameters.

Applying the SLIP model solely to the control of the knee joint offers two key advantages. Firstly, it enables the adjustment of the leg-lifting height via the desired virtual leg length, which not only enhances the robot's obstacle-crossing capability (as shown in Figure 16) but also reduces the impact force between the foot and the ground through the model's compliance. This compliance, in turn, improves the robot's locomotion efficiency, as evidenced in Table 6.

In this paper, we adopt a multi-model fusion strategy combining CPG-driven proximal joints with SLIP/VMC-controlled distal joints. Compared with the open-loop

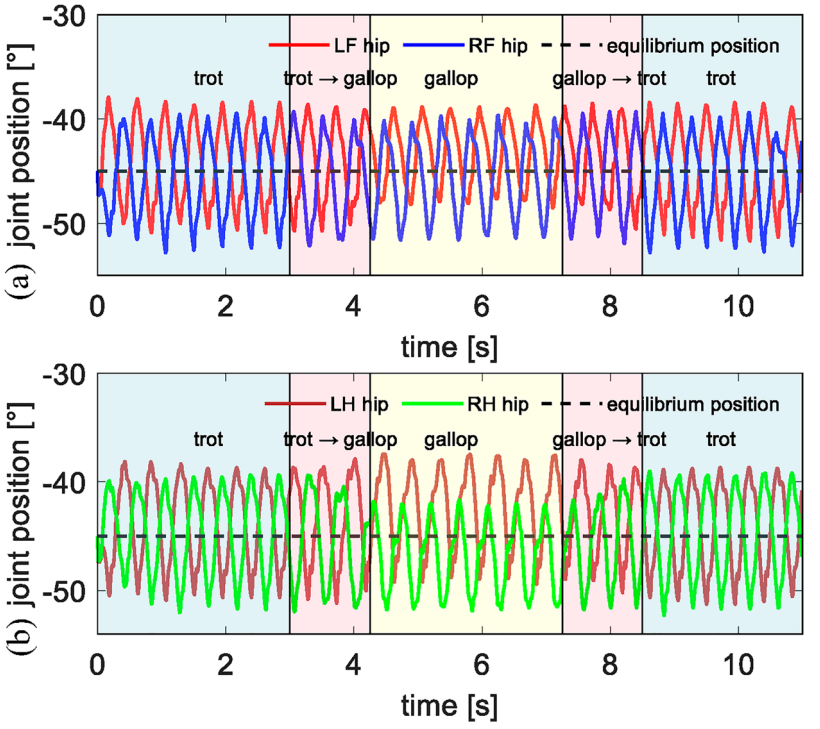

Figure 14. Gait transition with the 'FeiFei' robot. (a) and (j) are trotting. (b) and (c) are the transition from trotting to galloping. (d) ∼ (g) Galloping. (h) and (i) are the transition from galloping to trotting. Red curves mark the LF and RH legs, while green curves mark the RF and LH legs. Solid curves indicate the stance phase, and dashed curves indicate the swing phase. The orange arrow marks the walking direction.

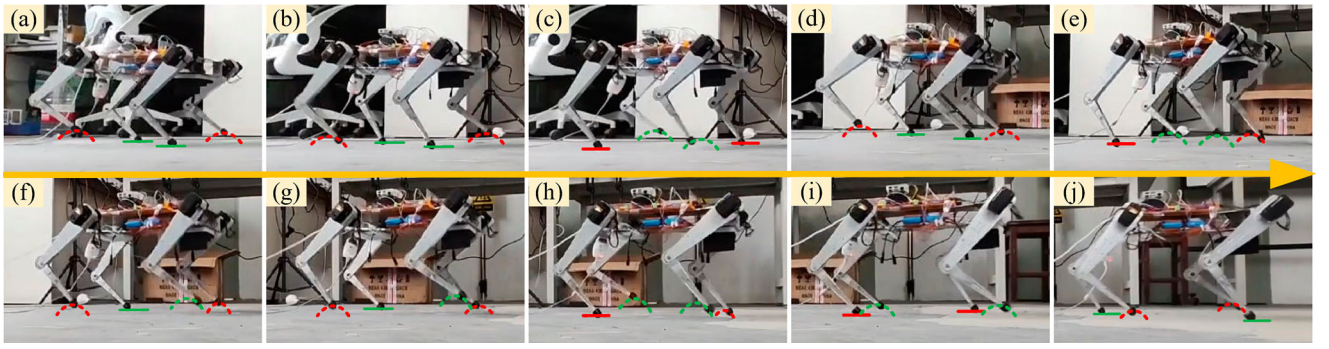

Figure 15. The actual angles of the hip joints of the four legs. (a) Front legs; (b) Hind legs. The gait transition process lasts for 11 seconds and the figure is accordingly divided into 5 regions.

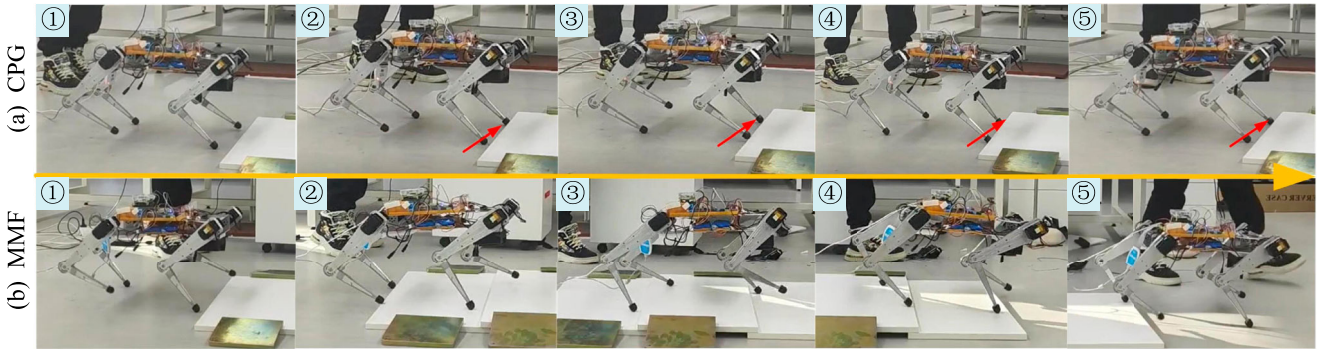

Figure 16. Walking crossing stepped terrains. (a) With CPG, the robot fails to step onto the platform, as indicated by the red arrow. (b) With MMF, it can smoothly walk across uneven terrains. The orange arrow marks the walking direction.

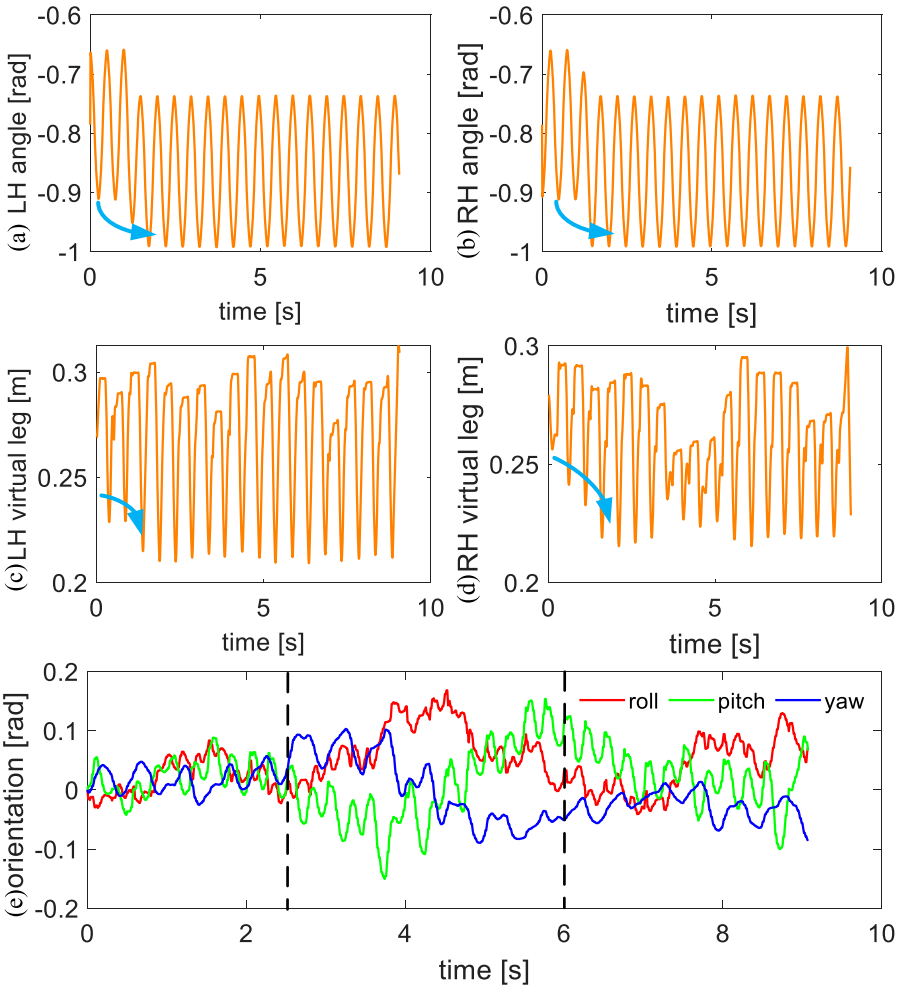

Figure 17. Locomotion trajectory for walking across uneven terrain. The blue arrow in (a) ∼ (d) indicates the trend of changes in the parameters. (a) and (b) plot the hip angles of LH and RH legs. (c) and (d) plot the virtual leg lengths of LH and RH legs. (e) plots the body orientation of the robot.

CPG control [1], our approach incorporates sensor feedback and torque control, thereby improving stability and energy efficiency in complex environments. Furthermore, this study demonstrates intrinsic consistency with Geyer et al.'s concept of 'muscle reflexes encoding legged mechanics principles'. Geyer et al. showed that local reflexes can effectively integrate mechanical stability and environmental adaptability by achieving stance leg compliance and swing leg coordination in human walking through positive force feedback (F+) and length feedback (L+) [34]. Building upon this framework, we translate biological reflex mechanisms into an engineered model: the spring-damping behaviour of distal joints is emulated via the SLIP model (analogous to Geyer's compliant leg dynamics), while establishing a hierarchical architecture of proximal active control coupled with distal compliant response through CPG-generated rhythms for proximal joints.

6. Conclusion

This work presents a bio-inspired multi-model fusion motion control approach for quadrupedal locomotion. In our approach, a high-stiffness rhythmic motion for the proximal hip joint is generated using a CPG. Then, to achieve low-stiffness knee movement, a finite state machine is formed based on the output of the CPG. On top of this, a SLIP model is used to derive the distal knee torque. To improve tracking performance and robustness, the parameters of the CPG system are adjusted online by incorporating sensory information, and VMC is also added for knee joint torque compensation. Hardware experiments are conducted on a quadrupedal robot. The results show that, compared to the traditional CPG method, the MMF method improves the robot's stability, increases the forward speed, and reduces energy consumption. With the proposed control method, the robot can also achieve smooth gait transition and traverse uneven terrains.

Due to limitations of the hardware platform, MMF is currently unable to be compared with model predictive control or reinforcement learning. In the future, we will optimize the hardware system of 'Feifei' by upgrading the leg structure from 2 degrees of freedom (DOF) to 3DOF, enabling full spatial motion capabilities, and apply the proposed controller to this enhanced robotic platform.

Disclosure statement

No potential conflict of interest was reported by the author(s).

Funding

This work was supported by the National Key R&D Program of China (Grant No.: KMB05322001534).

Notes on contributors

Jianing Wu obtained a Master of Engineering degree from Beijing Jiaotong University in 2025, with research interests including motion control and state estimation of quadruped robots.

Senwei Huang is a Ph.D. candidate at Beijing Jiaotong University, with his main research focus on the motion control of bio-inspired quadruped robots.

Xiuli Zhang obtained her PhD in Mechanical Engineering from Tsinghua University in 2004. In 2005, she served as a research assistant at the Hong Kong University of Science and Technology. In 2013, she was a visiting scholar at the University of Michigan. She is currently an associate professor at the School of Mechanical and Electronic Control Engineering, Beijing Jiaotong University, and the head of the Bio-inspired Intelligent Robot Research Group. Her main research interests include bionic control technology for quadruped robots and brain-inspired learning algorithms for humanoid robots.

Jiatao Ding received his B.Eng. and Ph.D. degrees in Engineering from Wuhan University, China, in 2014 and 2020, respectively. From 2018–2020, he was a visiting Ph.D. student at the Italian Institute of Technology, Italy. From 2020–2022, he worked as an assistant research scientist at the Shenzhen Institute of Artificial Intelligence and Robotics for Society, China. From 2022-2025, he was a Postdoctoral Researcher with the Department of Cognitive Robotics, Delft University of Technology, The Netherlands. He is currently a Senior Postdoctoral Researcher with the Department of Industrial Engineering, University of Trento, Italy. His research interests include optimal control and robot learning on legged locomotion.

References

[1] Go E, Lee JH, Kim SY, et al. Stakeholder perspectives on safety issues in collaborative mobile robots: a case study of quadruped robot applications in a smart factory. Appl Sci. 2024;14(22):10232. doi: 10.3390/app142210232

[2] Schneider L, Frey J, Miki T. Learning risk-aware quadrupedal locomotion using distributional reinforcement learning. In: 2024 IEEE International Conference on Robotics and Automation, Yokohama, Japan; 2024. p. 11451–11458.

[3] Ding J, Posthoorn P, Atanassov V, et al. Quadrupedal locomotion with parallel compliance: E-go design, modeling, and control. IEEE ASME Trans Mechatron. 2024;29(4): 2839–2848. doi: 10.1109/TMECH.2024.3402321

[4] Li W, Zhou Z, Cheng H. Dynamic locomotion of a quadruped robot with active spine via model predictive control. In: 2023 IEEE International Conference on Robotics and Automation, London, UK; 2023. p. 1185–1191.

[5] Grandia R, Jenelten F, Yang S, et al. Perceptive locomotion through nonlinear model-predictive control. IEEE Trans Robot. 2023;39(5):3402–3421. doi: 10.1109/TRO.2023.3275384

[6] Ding J, Atanassov V, Panichi E, et al. Robust quadrupedal jumping with impact-aware landing: exploiting parallel elasticity. IEEE Trans Robot. 2024;40:3212–3231. doi: 10.1109/TRO.2024.3411988

[7] Kim D, Di Carlo J, Katz B, et al. Highly dynamic quadruped locomotion via whole-body impulse control and model predictive control. Preprint; 2019. Available at arXiv:190906586.

[8] Liao Q, Li Z, Thirugnanam A. Walking in narrow spaces: safety-critical locomotion control for quadrupedal robots with duality-based optimization, Detroit, MI, USA; 2023. p. 2723–2730.

[9] Morlando V, Teimoorzadeh A, Ruggiero F. Whole-body control with disturbance rejection through a momentum-based observer for quadruped robots. Mech Mach Theory. 2021;164:104412. doi: 10.1016/j.mechmachtheory.2021.104412

[10] Miki T, Lee J, Hwangbo J. Learning robust perceptive locomotion for quadrupedal robots in the wild. Sci Rob. 2022;7(62):eabk2822. doi: 10.1126/scirobotics.abk2822

[11] Jeon S, Jung M, Choi S, et al. Learning whole-body manipulation for quadrupedal robot. IEEE Rob Autom Lett. 2023;9(1):699–706. doi: 10.1109/LRA.2023.3335777

[12] Bellegarda G, Nguyen C, Nguyen Q. Robust quadruped jumping via deep reinforcement learning. Rob Auton Syst. 2024;182:104799. doi: 10.1016/j.robot.2024.104799

[13] Han L, Zhu Q, Sheng J, et al. Lifelike agility and play in quadrupedal robots using reinforcement learning and generative pre-trained models. Nature Machine Intell. 2024;6(7):787–798. doi: 10.1038/s42256-024-00861-3

[14] Atanassov V, Ding J, Kober J, et al. Curriculum-based reinforcement learning for quadrupedal jumping: a reference-free design. Preprint; 2024. Available at arXiv:240116337.

[15] Imai CS, Zhang M, Zhang Y. Vision-guided quadrupedal locomotion in the wild with multi-modal delay randomization, Kyoto, Japan; 2022. p. 5556–5563.

[16] Marder E, Bucher D. Central pattern generators and the control of rhythmic movements. Curr Biol. 2001;11(23): R986–R996. doi: 10.1016/S0960-9822(01)00581-4

[17] Ijspeert AJ. Central pattern generators for locomotion control in animals and robots: a review. Neural Netw. 2008;21(4):642–653. doi: 10.1016/j.neunet.2008.03.014

[18] Rutishauser S, Sprowitz A, Righetti L. Passive compliant quadruped robot using central pattern generators for locomotion control, Scottsdale, AZ, USA; 2008. p. 710–715.

[19] Yu H, Gao H, Deng Z. Enhancing adaptability with local reactive behaviors for hexapod walking robot via sensory

feedback integrated central pattern generator. Rob Auton Syst. 2020;124:103401. doi: 10.1016/j.robot.2019.103401

[20] Ajallooeian M, Gay S, Tuleu A. Modular control of limit cycle locomotion over unperceived rough terrain, Tokyo, Japan; 2013. p. 3390–3397.

[21] Bellegarda G, Ijspeert A. Cpg-rl: learning central pattern generators for quadruped locomotion. IEEE Rob Autom Lett. 2022;7:12547–12554. doi: 10.1109/LRA.2022.3218167

[22] Fukui T, Fujisawa H, Otaka K, et al. Autonomous gait transition and galloping over unperceived obstacles of a quadruped robot with CPG modulated by vestibular feedback. Rob Auton Syst. 2019;111:1–19. doi: 10.1016/j.robot.2018.10.002

[23] Saputra AA, Ijspeert AJ, Kubota N. A neural primitive model with sensorimotor coordination for dynamic quadruped locomotion with malfunction compensation, Las Vegas, NV, USA; 2020. p. 3783–3788.

[24] Herneth C, Hayashibe M, Owaki D. Learnable tegotae-based feedback in cpgs with sparse observation produces efficient and adaptive locomotion, London, UK; 2023. p. 1155–1161.

[25] Bellegarda G, Shafiee M, Ijspeert A. Visual cpg-rl: Learning central pattern generators for visually-guided quadruped locomotion, Yokohama, Japan; 2024. p. 1420–1427.

[26] Bellegarda G, Shafiee M, Özberk ME, et al. Quadruped-frog: rapid online optimization of continuous quadruped jumping. Preprint; 2024. Available at arXiv:240306954.

[27] Donelan J, Pearson K. Contribution of force feedback to ankle extensor activity in decerebrate walking cats. J. Neurophysiol.. 2004;92(4):2093–2104. doi: 10.1152/jn.00325.2004

[28] Daley MA, Felix G, Biewener AA. Running stability is enhanced by a proximo-distal gradient in joint neuromechanical control. J. Experimental Biol.. 2007;210(3):383–394. doi: 10.1242/jeb.02668

[29] Ijspeert AJ, Daley MA. Integration of feedforward and feedback control in the neuromechanics of vertebrate locomotion: a review of experimental, simulation and robotic studies. J. Experimental Biol.. 2023;226(15):jeb245784. doi: 10.1242/jeb.245784

[30] Liu H, Jia W, Bi L. Hopf oscillator based adaptive locomotion control for a bionic quadruped robot, Takamatsu, Japan; 2017. p. 949–954.

[31] Raibert MH. Legged robots that balance. Cambridge, MA: MIT Press; 1986.

[32] Fan Y, Pei Z, Wang C, et al. A review of quadruped robots: structure, control, and autonomous motion. Advanced Intelligent Systems. 2024;6:2300783. doi: 10.1002/aisy.v6.6

[33] Bloesch M, Hutter M, Hoepflinger MA, et al. State estimation for legged robots-consistent fusion of leg kinematics and imu. Robotics. 2013;17:17–24. doi: 10.7551/mitpress/9816.001.0001

[34] Geyer H, Herr H. A muscle-reflex model that encodes principles of legged mechanics produces human walking dynamics and muscle activities. IEEE Trans Neural Syst Rehabil Eng. 2010;18(3):263–273. doi: 10.1109/TNSRE.7333